Cell-Specific Information Processing in Segregating Populations of Eph Receptor Ephrin –Expressing Cells

Claus Jørgensen, *et al.*

Science **326**, 1502 (2009);
DOI: 10.1126/science.1176615

Cell-Specific Information Processing in Segregating Populations of Eph Receptor Ephrin–Expressing Cells

Claus Jørgensen,[1] Andrew Sherman,[1,2] Ginny I. Chen,[1,2] Adrian Pasculescu,[1] Alexei Poliakov,[3] Marilyn Hsiung,[1] Brett Larsen,[1] David G. Wilkinson,[3] Rune Linding,[4]* Tony Pawson[1,2]*

Cells have self-organizing properties that control their behavior in complex tissues. Contact between cells expressing either B-type Eph receptors or their transmembrane ephrin ligands initiates bidirectional signals that regulate cell positioning. However, simultaneously investigating how information is processed in two interacting cell types remains a challenge. We implemented a proteomic strategy to systematically determine cell-specific signaling networks underlying EphB2- and ephrin-B1–controlled cell sorting. Quantitative mass spectrometric analysis of mixed populations of EphB2- and ephrin-B1–expressing cells that were labeled with different isotopes revealed cell-specific tyrosine phosphorylation events. Functional associations between these phosphotyrosine signaling networks and cell sorting were established with small interfering RNA screening. Data-driven network modeling revealed that signaling between mixed EphB2- and ephrin-B1–expressing cells is asymmetric and that the distinct cell types use different tyrosine kinases and targets to process signals induced by cell-cell contact. We provide systems- and cell-specific network models of contact-initiated signaling between two distinct cell types.

Signal transduction is typically studied by the stimulation of target cells with a soluble extracellular ligand, such as a growth factor (*1*). However, this approach does not necessarily recapitulate the physiological process of intercellular communication, in part because protein ligands for some transmembrane receptors may themselves be attached to the surface of cells. Furthermore, signaling initiated by cell-cell contact is typically a reciprocal process, in which two cell types exchange distinct signals, leading to mutually dependent alterations in their respective behaviors. For example, events such as axon guidance, antigen presentation, and generation of apical-basal polarity can involve two or more cells that directly interact through membrane-tethered receptors to exchange signaling information (*2*). In particular, direct interactions between transmembrane Eph receptor tyrosine kinases (EphRs) and their membrane-bound ephrin ligands frequently lead to mutual cell repulsion and are important for axon guidance and boundary formation during tissue development (*3*–*6*).

EphRs, which make up the largest family of mammalian receptor tyrosine kinases, bind cell surface–associated ephrins that have either a glycosylphosphatidylinositol (GPI) membrane anchor (A-type ephrins) or a transmembrane region followed by a conserved cytoplasmatic tail (B-type ephrins). Clustering of B-type EphRs and ephrins at the surface of adjacent cells activates phosphotyrosine (pTyr) signaling in both the EphR- and ephrin-expressing cells, termed forward and reverse signaling, respectively (*7*–*9*). Ephrins lack intrinsic catalytic activity, and reverse signaling is achieved through the activation of associated tyrosine kinases and direct binding of intracellular targets (*10*, *11*). Analysis of EphR or ephrin signaling initiated with artificial soluble ligands provides limited understanding of the cell-specific signaling networks (*6*, *12*) because signaling between neighboring EphR- and ephrin-expressing cells may also be affected by inputs from adhesion molecules and the extracellular matrix (*6*, *13*, *14*). We therefore set out to identify cell-specific responses, including quantitative differences between the underlying multivariate signaling networks in the two cell types (*15*, *16*).

Systematic analysis of cell-specific networks in distinct populations of interacting cells is challenging primarily because the unique properties of each cell type are lost once cocultured cells are processed for biochemical analysis, such as by immunoblotting. Thus, to investigate bidirectional EphR-ephrin signaling in the context of direct cell-cell interactions we developed a proteomic strategy termed quantitative analysis of Bidirectional Signaling (qBidS), which is based on lineage-specific labeling with stable isotopomeric versions of amino acids (SILAC), specifically arginine and lysine, combined with mass spectrometric identification and relative quantification of tyrosine-phosphorylated peptides. Systematic evaluation of mixed populations of EphR- and ephrin-expressing cells with this approach was then combined with a phenotypic analysis of EphR- and ephrin-dependent cell sorting by means of small interfering RNA (siRNA) screening and data-driven computational modeling of signaling networks. This identified extensive cell-specific information processing as well as asymmetric network structure and utilization during bidirectional signaling between EphB2- and ephrin-B1–expressing cells.

Quantitative analysis of bidirectional Eph receptor–ephrin signaling. To study bidirectional EphR-ephrin signaling, we used human embryonic kidney (HEK) 293 cell lines engineered to express either EphB2 (EphB2$^+$ cells) or ephrin-B1 (ephrin-B1$^+$ cells) (figs. S1 and S2) (*17*, *18*). These cells show a repulsive response when they contact one another in cell culture and display self-organizing properties so that the EphB2$^+$ cells, which are marked with a membrane-targeted myristoylated green fluorescent protein (GFP), form multicellular colonies with sharp boundaries that exclude ephrin-B1$^+$ cells. To quantitatively investigate the response of signaling networks in either EphB2$^+$ or ephrin-B1$^+$ cells, we used SILAC (*19*, *20*) to differentially label the two cell types.

EphB2$^+$ cells were grown independently in the presence of "light" (C12N14) arginine and lysine or with "heavy" (C13N15) arginine and lysine (*21*). Ephrin-B1$^+$ cells were labeled separately with "medium" (C12N15) arginine and lysine (Fig. 1A). The incorporation of these amino acids into the proteins of each cell line enabled relative quantification of signaling events in a cell line–specific manner (Fig. 1, A and B). To initiate signaling by cell-cell contact, medium-labeled ephrin-B1$^+$ cells were combined with the adherent heavy-labeled EphB2$^+$ cells. After 10 min, the cells were lysed under denaturing conditions and mixed with light-labeled, nonstimulated EphB2$^+$ cells as a point of reference (Fig. 1A). Tyrosine-phosphorylated peptides were isolated and analyzed with liquid chromatography-mass spectrometry (LC-MS) on an LTQ-Orbitrap (Thermo Scientific, San Jose, California) (*18*, *22*, *23*). The peptide data are available at www.ephomics.org.

Because peptides with identical sequences but originating from distinct cell lines differ by the mass differences resulting from the SILAC labeling, their relative abundance can be determined by comparing their extracted ion currents (Fig. 1B). This enables quantification of protein phosphorylation specific to the EphB2$^+$ cells by using the ratio between heavy-labeled peptides (EphB2$^+$, stimulated) and the corresponding light-labeled peptides (EphB2$^+$, control). At the same time, peptides originating from ephrin-B1$^+$ cells that were used for stimulation can be distinguished by their medium labeling (Fig. 1, B and C). As examples, we observed that phosphorylation of the activation loop of EphB2 (Y780) was increased by 80% after mixing EphB2$^+$ and ephrin-B1$^+$ cells. Conversely, a tyrosine-phosphorylated peptide from the intracellular region of ephrin-B1 (Y317)

[1]Samuel Lunenfeld Research Institute (SLRI), Mount Sinai Hospital, Toronto M5G 1X5, Canada. [2]Department of Molecular Genetics, University of Toronto, Toronto M5S 1A8, Canada. [3]Division of Developmental Neurobiology, Medical Research Council (MRC) National Institute for Medical Research (NIMR), London NW7 1AA, UK. [4]Cellular & Molecular Logic Team, Section of Cell and Molecular Biology, Institute of Cancer Research (ICR), London SW3 6JB, UK.

*To whom correspondence should be addressed. E-mail: linding@icr.ac.uk (R.L.); pawson@lunenfeld.ca (T.P.)

was only observed with the medium label, showing that it specifically originated from the ephrin-B1$^+$ cell population. We identified pTyr sites in previously described EphB2 targets, such as the PDZ domain–containing protein Afadin [AF6 (Y1657)] and the adaptor protein SHC1 (Y427), both of which were threefold more abundant in the stimulated EphB2$^+$ cell population (Fig. 1C). The experimental approach was then reversed so as to identify dynamic pTyr signaling in ephrin-B1$^+$ cells mixed with EphB2$^+$ cells (fig. S3) (*18*).

Bidirectional signaling between EphB2- and ephrin-B1–expressing cells is asymmetric. Analysis of the global changes in tyrosine phosphorylation induced by contact between EphB2$^+$ and ephrinB1$^+$ cells identified a total of 442 tyrosine phosphorylation sites on 304 target proteins that significantly increased or decreased in abundance in one or both cell types ($P < 0.05$; Wilcoxon test) (table S1) (*18*). Contact-initiated signaling between EphB2$^+$ and ephrin-B1$^+$ cells affected pTyr sites from proteins with a wide range of cellular functions and revealed both known and previously undescribed targets (Fig. 2A and fig. S4). These include regulators of adhesion, polarity, phosphoinositide signaling, actin remodeling, endocytosis, and cell-cell interactions, implicating these cellular processes in the regulation of EphR-ephrin–controlled cell sorting.

To quantitatively assess cell-specific signaling events, and to avoid sampling bias from the MS analysis, we identified identical peptides that were tyrosine-phosphorylated in both EphB2$^+$ and ephrin-B1$^+$ cells and compared their dynamic profiles between the two cell types. Overall, these profiles revealed a shifted distribution ($P < 1 \times 10^{-36}$; Wilcoxon test) (fig. S5A), confirming that the responses initiated by cell-cell contact differ between the distinct cell populations. We compared the cell-specific modulation of the 100 common tyrosine phosphorylation sites, which we grouped according to the signaling domains present on the phosphorylated proteins (Fig. 2B). Of these sites, 71% displayed asymmetric modulation between the cell lines ($P < 0.05$; Wilcoxon test). Adaptor proteins such as SHB, SHC1, and DOK1 displayed significantly increased tyrosine phosphorylation in stimulated EphB2$^+$ cells, whereas in ephrin-B1$^+$ cells the phosphorylation of these sites was decreased ($P < 0.05$; Wilcoxon test). The phosphorylation of focal adhesion kinase [PTK2 (Y576 and Y577)] and paxillin [PXN (Y118)] was increased in both EphB2$^+$ and ephrin-B1$^+$ cells but to a significantly higher extent in the ephrin-B1$^+$ cells ($P < 0.05$; Wilcoxon test). Thus, the observed asymmetry is not simply due to a more general increase in tyrosine kinase activity in the EphB2$^+$ cells. A third group of pTyr sites was similarly modulated in both EphB2$^+$ and ephrin-B1$^+$ cells; for example, phosphorylation of Y2645 on adenomatous polyposis coli (APC) was decreased to a similar extent in both cell types, whereas phosphorylation of Y15 on cyclin-dependent kinase 5 (CDK5) was similarly increased in both EphB2$^+$ and ephrin-B1$^+$ cells ($P > 0.85$; Wilcoxon test). Thus, signaling networks induced by contact between EphB2$^+$ and ephrin-B1$^+$ cells show both cell-specific and shared modes of regulation. Preferential pTyr modulation of adaptor proteins in EphB2$^+$ cells suggests that these docking proteins probably have cell-specific regulatory functions. Examination of all significantly modulated pTyr sites revealed an overall increase in tyrosine phosphorylation of proteins containing Src homology 2 domain (SH2), Src homology 3 domain (SH3), or tyrosine kinase domains in EphB2$^+$ cells as compared with those in ephrin-B1$^+$ cells (fig. S6) (*18*).

Functional analysis of cell-sorting through siRNA screening. The quantitative analysis of tyrosine phosphorylation events during EphB2 and ephrin-B1 bidirectional signaling marks the activation state of signaling networks in the interacting cell populations. In order to relate these phosphoproteomic results to the phenotypic response of cell sorting and to obtain functional data for the modeling of cellular signal processing, we used an siRNA screen to analyze the role of selected signaling proteins in EphB2- and ephrin-B1–mediated cell segregation (Fig. 3). To this end, EphB2$^+$ cells and ephrin-B1$^+$ cells were mixed, transfected with siRNA, and grown to confluence (*18*). Whereas mixed control populations of EphB2$^+$ and ephrin-B1$^+$ cells formed distinct colonies with well-defined boundaries (fig. S7), transfection with siRNAs targeting EphB2 or ephrin-B1 significantly decreased the numbers of segregated GFP-positive colonies, indicating that cell sorting is a robust assay for EphB2–ephrin-B1 function (Fig. 3A and fig. S8).

We used a custom library of 2172 siRNA pools [SMARTpools (Dharmacon, Thermo Scientific, Lafayette, Colorado)] directed against targets with selected signaling domains, including kinases, phosphatases, and pTyr recognition modules (table S4), to screen for proteins involved in cell sorting (Fig. 3 and fig. S9B) (*18*). We analyzed the number of resulting EphB2$^+$ GFP-positive colonies by means of automated microscopy on an Arrayscan II (Cellomics, Thermo Scientific, Pittsburgh, Pennsylvania) (fig. S9A) and identified 589 siRNAs that significantly affected

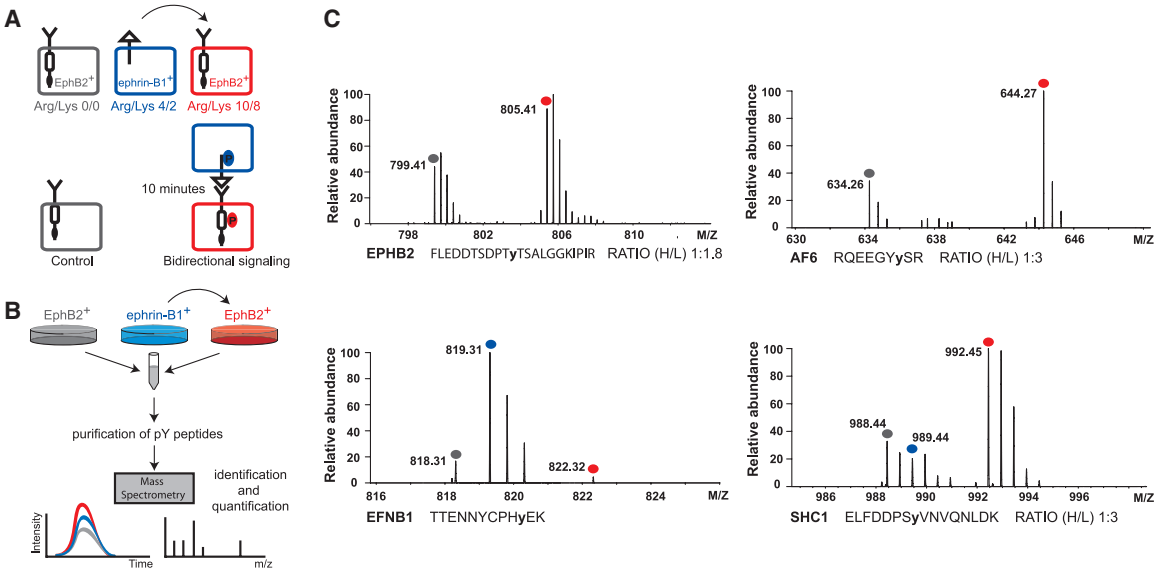

Fig. 1. Experimental outline of qBidS. (**A**) Cell-specific signaling in mixed populations of EphB2$^+$ and ephrin-B1$^+$ cells. EphB2$^+$ cells were labeled with light or heavy arginine and lysine, and ephrin-B1$^+$ cells were labeled with medium arginine and lysine. Bidirectional signaling was initiated, and nonstimulated light-labeled EphB2$^+$ cells served as a control. (**B**) Mixed populations of cells were harvested after 10 min and combined with nonstimulated control cells. Cell lysates were digested with trypsin, and tyrosine-phosphorylated peptides were isolated and analyzed with LC-MS on a LTQ-Orbitrap. (**C**) Peptides from mixed-cell populations were differentiated and quantified via their distinct isotopic labels. In EphB2$^+$ cells mixed with ephrin-B1$^+$ cells, phosphorylation of the activation loop of EPHB2 at Y780 was increased by 80%, as determined from the ratio of heavy- to light-labeled peptides. Tyrosine phosphorylation of ephrin-B1 (Y317) was only observed with a medium label, indicating that this peptide originates specifically from the ephrin-B1$^+$ cells. The previously described EphB2 targets AF6 (Y1657) and SHC1 (Y427) display threefold increased levels of phosphorylation in the heavy-labeled EphB2$^+$ cell population.

colony formation (the mock transfection averaged 90 colonies ± 15 within each biological replicate; $n = 4$ biological replicates) (figs. S8 and S9) (*18*). All affected cultures were then visually inspected, and 237 siRNAs that affect growth and adhesion were discarded. Off-target effects are inherent to siRNA technology (*24*), so we reanalyzed the remaining 352 targets with four individual siRNAs [ON-TARGETplus (OTP) reagents (Dharmacon, Thermo Scientific, Lafayette, Colorado)] that were distinct from those used in the initial screen and applied them to each target. Cocultures in which siRNAs recapitulated a significant effect on colony numbers were also visually confirmed (*18*). This approach yielded 200 targets that affect EphB2- and ephrin-B1–dependent cell sorting (fig. S8D and table S3), including several previously described effectors of EphR and ephrin signaling, such as p120RasGAP (RASA1) and the adaptor proteins CRK and NCK2. The screen also identified groups of multiple interacting proteins that potentially have a coordinated role in the regulation of aspects of EphB2–ephrin-B1 cell sorting, such as cytoskeletal organization and cell adhesion (fig. S9C). For example, activators (DOCK1 and ELMO) as well as negative regulators (CHN1 and CHN2) of RAC1 guanosine triphosphatase (GTPase) activity, in addition to RAC1 itself, were identified as targets, which suggests that tight control of RAC1 activity is important for cell sorting.

We then compared the targets identified in the siRNA screen with those containing pTyr sites modulated by the mixing of EphB2$^+$ and ephrin-B1$^+$ cells. Among the 200 proteins required for proper cell sorting, 37 were significantly modulated by tyrosine phosphorylation in EphB2$^+$ cells and 26 in ephrin-B1$^+$ cells (fig. S8E and table S3), of which 18 were significantly modulated in both cell types by phosphorylation on identical tyrosine sites (Fig. 3B and fig. S8E). These proteins identified in both the siRNA and qBidS screens have a wide range of molecular and cellular functions and include adaptor proteins (SHB and SHC1), kinases (ABL1 and EPHB2), phospholipid regulators (SHIP-2 and PLCG2), polarity proteins (PARD3, DLG3, and APC), and regulators of the cytoskeleton, endocytosis, and migration (PTK2, PXN, WASL, and ITSN2) (Fig. 3B and table S3), highlighting the role of these cellular processes in the regulation of EphR-ephrin–controlled cell sorting. The pTyr sites from the 18 targets modulated in both cell types nonetheless displayed significant differences in their cell-specific modulation ($P = 0.008$; Fisher's exact test) (fig. S9D), indicating that asymmetric tyrosine phosphorylation affects proteins that are essential for cell sorting.

Thus, EphB2- and ephrin-B1–affected changes in tyrosine phosphorylation elicit extensive changes in intracellular signaling networks. Therefore, we set out to derive a network model of cell-specific information flow on the basis of the quantified modulation of tyrosine phosphorylation and the targets identified in the siRNA screen for cell sorting.

Modeling of cell-specific dynamic networks during cell-sorting. The regulation of tyrosine phosphorylation through activated kinases and subsequent binding of pTyr sites by domains like SH2 and PTB (pTyr-binding) creates molecular circuitries (*25*, *26*) that underlie cellular decision-making. The information flow within such a system can therefore be visualized by assigning kinases, phosphatases, and phospho-binding modules for each pTyr site (kinase/phosphatase → substrate/site → phospho-binding domain). For example, increased phosphorylation of Tyr sites can be correlated with an increased activity of the associated kinase or kinases (or decreased activity

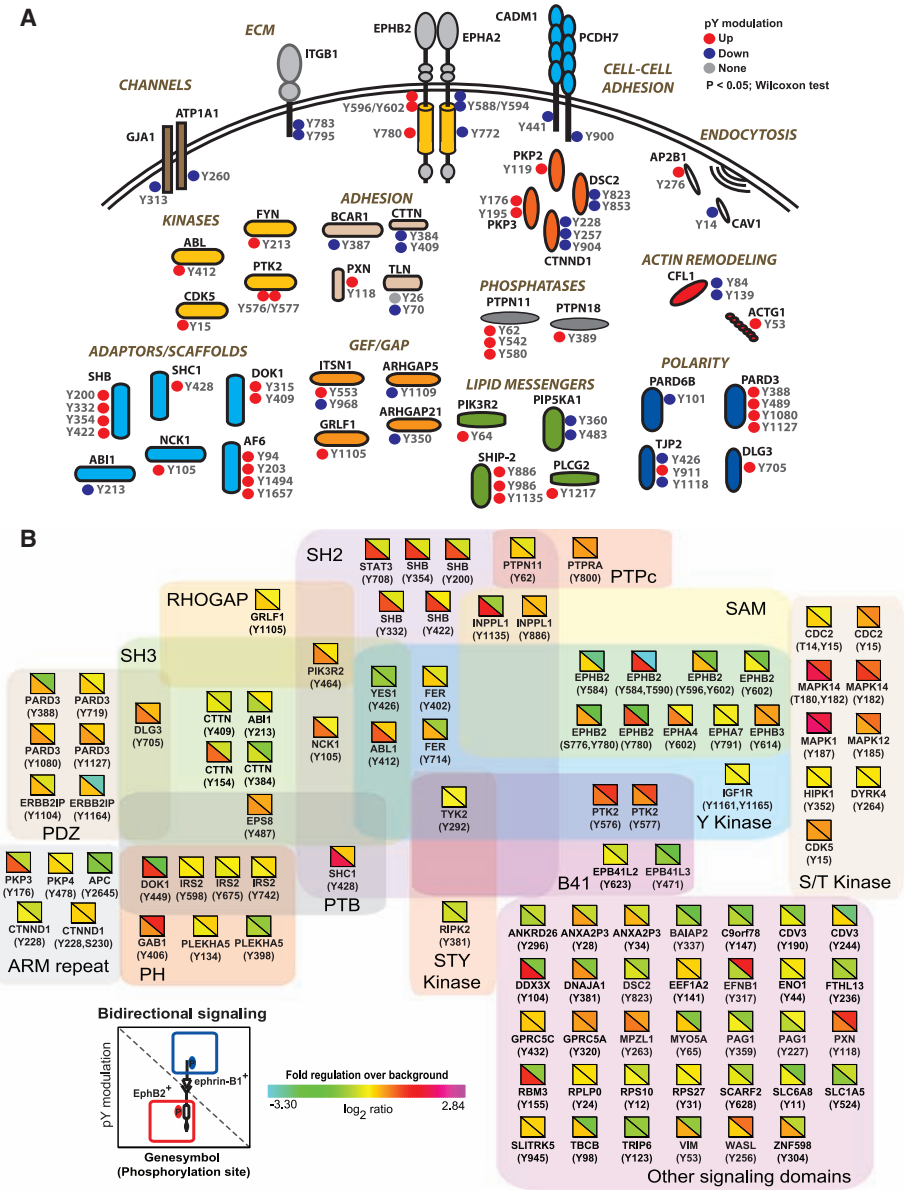

Fig. 2. Asymmetric regulation of tyrosine phosphorylation in EphB2$^+$ and ephrin-B1$^+$ cells. (**A**) Overview of selected proteins in EphB2$^+$ cells modulated by tyrosine phosphorylation after mixing with ephrin-B1$^+$ cells. The modulation of pTyr sites is indicated as significantly increased (red), not modulated (gray), or decreased (blue). Molecules that are involved in a wide variety of cellular functions, such as lipid signaling (SHIP-2, PLCG2, and PIK3R2), polarity (DLG3 and PARD3), actin and myosin turnover (NCK1 and ACTG1), endocytosis and recycling (AP2B1 and CAV1), and adaptor proteins (SHB and SHC1), as well as kinases (ABL1 and CDK5) are modulated by tyrosine phosphorylation, indicating that phospho-regulation of numerous cellular processes may be important for cell sorting. (**B**) Comparison of contact-initiated pTyr signaling between ephrin-B1$^+$ and EphB2$^+$ cells. Identical pTyr sites are shown grouped according to the domain composition of their host proteins. Cell-specific modulation of pTyr sites is indicated by slashed boxes, each triangle representing specific regulation within EphB2$^+$ (bottom triangles) or ephrin-B1$^+$ (top triangles) cells, respectively. The fold regulation of each pTyr site is shown with a color range. In total, we identified 100 identical tyrosine-phosphorylated sites in the two cell types, of which 71 displayed asymmetric modulation between EphB2$^+$ and ephrin-B1$^+$ cells ($P < 0.05$; Wilcoxon test).

of a phosphatase). This increase will in turn enhance the association between phosphorylated sites and proteins that contain the appropriate phospho-binding domain (*27*). To model the bidirectional signaling networks in EphB2$^+$ and ephrin-B1$^+$ cells, we used the NetworKIN and NetPhorest algorithms [http://NetworKIN.info and http://NetPhorest.info (*28*, *29*)] to computationally reconstruct phosphorylation networks using probabilistic contextual data in combination with sequence models of kinase and phospho-binding domain consensus motifs (*28*, *29*). We identified pTyr sites from singly phosphorylated peptides common to the two cell types that exhibited significant modulation after cell-cell contact ($P < 0.05$; Wilcoxon test). Accurate modeling of phosphorylation networks requires contextual information for both kinases and substrates (*28*). Therefore, we developed four filtering steps to restrict the predicted kinases and phospho-binding proteins to those more likely to be relevant for cocultured EphB2–ephrin-B1–expressing HEK293 cells and to limit spurious predictions: First, predicted kinases or phospho-binding proteins were accepted only if they had been previously identified by the qBidS or siRNA screens (Fig. 4). Second, we required that kinases and substrates, which were predicted to interact, were similarly modulated (up, down, or none) (Fig. 4, co-modulation). The activities of kinases were determined by the modulation of their activation loop phosphorylation sites and correlated to the phosphorylation of substrate sites. Third, predictions were ranked and filtered on the basis of their probability from NetPhorest (Fig. 4) (*18*, *29*). We also analyzed the predicted kinase-substrate-target relationships by overlaying a HEK293-specific contextual network (Fig. 4) (*18*). The latter was generated with proteins identified through qBidS, siRNA screening, or coimmunoprecipitation with selected network proteins (table S5) (*18*) as seed input data to the Search

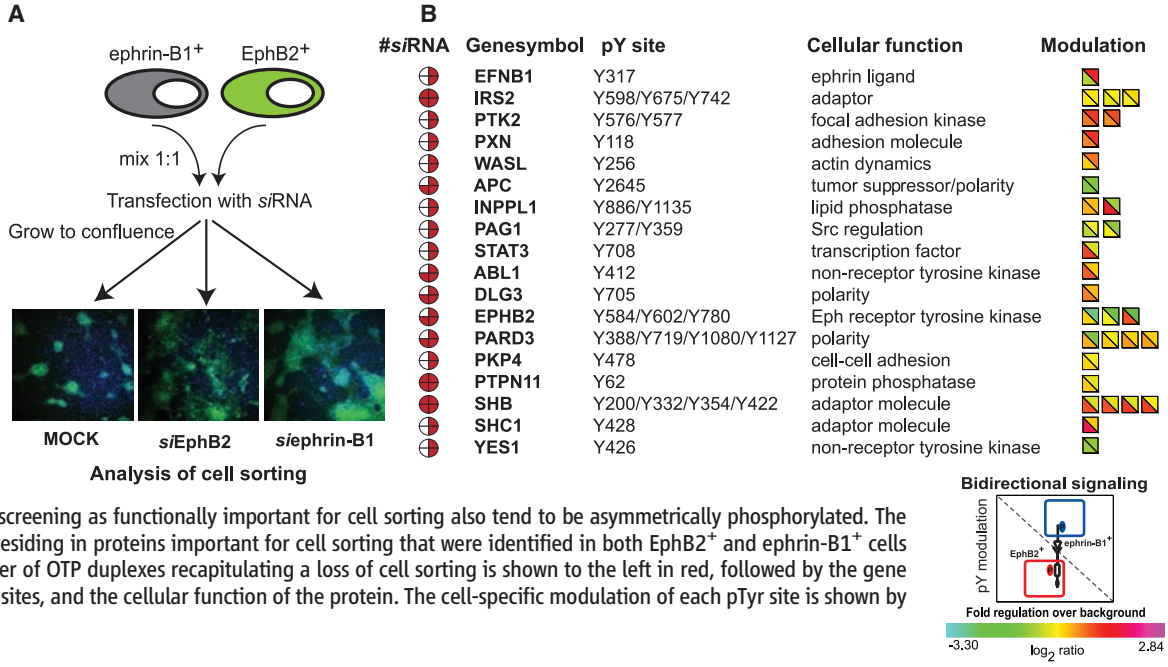

Fig. 3. Functional siRNA screening of EphB2- and ephrin-B1–regulated cell sorting. (**A**) EphB2$^+$ cells, which coexpress myristoylated GFP, were mixed with ephrin-B1$^+$ cells, transfected with siRNA pools, and grown to 100% density. The number of GFP-positive EphB2$^+$ colonies was used to determine the effect of siRNAs on cell sorting. Disruption of EphB2 or ephrin-B1 expression by means of siRNA inhibits colony formation. (**B**) Proteins identified through siRNA screening as functionally important for cell sorting also tend to be asymmetrically phosphorylated. The modulation of pTyr sites residing in proteins important for cell sorting that were identified in both EphB2$^+$ and ephrin-B1$^+$ cells was compared. The number of OTP duplexes recapitulating a loss of cell sorting is shown to the left in red, followed by the gene name, the identified pTyr sites, and the cellular function of the protein. The cell-specific modulation of each pTyr site is shown by color code.

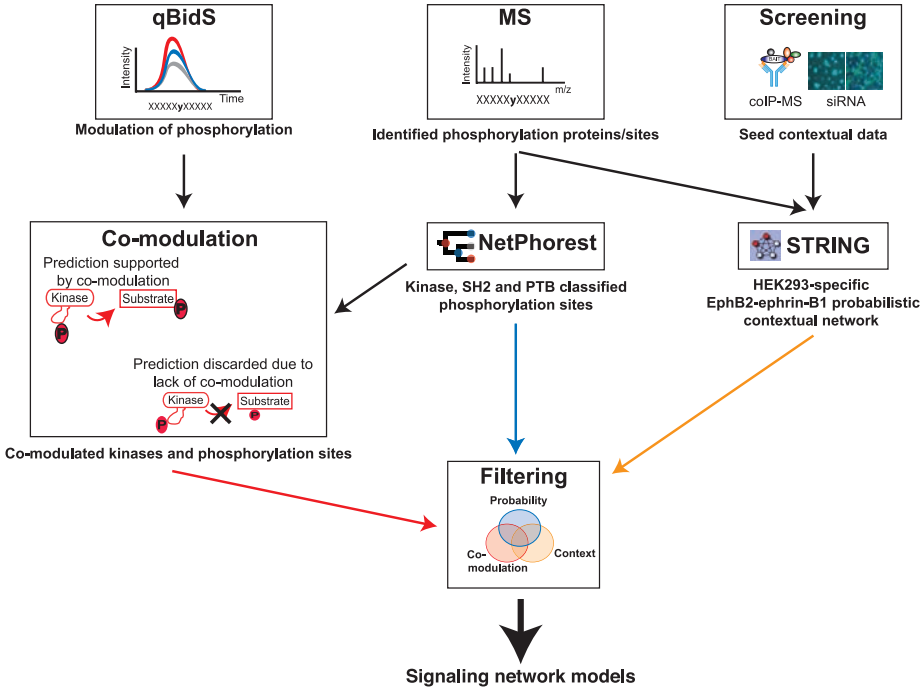

Fig. 4. Computational data integration and network modeling. Systems-specific data integration was performed to construct network models. All observed phosphorylation sites were first processed by the NetPhorest algorithm (*29*) so as to predict kinase-substrate relationships and SH2 and PTB domain interactions. These predictions were subjected to several subsequent filtering schemes: First, we required that tyrosine phosphorylation sites and the activation loop phosphorylation of their predicted kinases be comodulated (red path). Second, predictions were filtered on the basis of the probability score from Netphorest (blue path). Proteins that were identified through qBidS or siRNA screening or by coprecipitation were used as input to the STRING resource to generate a systems-specific protein-protein interaction network, permitting contextual filtering (orange path) similar to the NetworKIN algorithm (*28*). This enabled the generation of cell-specific signaling network models.

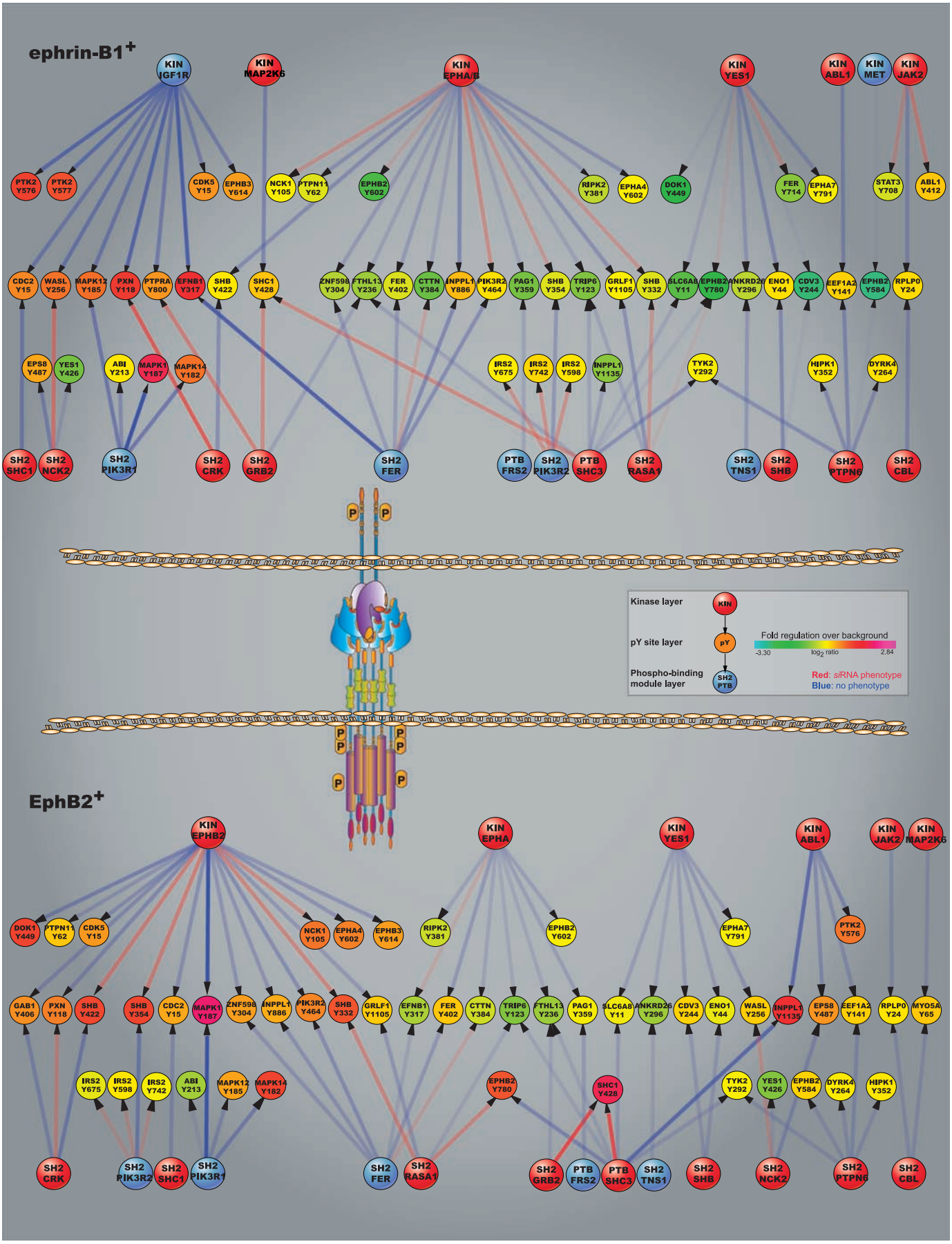

Fig. 5. Cell-specific signaling network models in EphB2- and ephrin-B1–expressing cells. Cell-specific information flow in EphB2$^+$ and ephrin-B1$^+$ cells is shown in the form of modular protein networks with kinases (KIN), pTyr sites, and phospho-binding modules (SH2 and PTB) organized in layers. The predicted kinases and phospho-binding modules for each tyrosine-phosphorylated residue are shown. The color of the pTyr sites represents their cell-specific modulation, according to the indicated color code, whereas the color of each kinase and phospho-binding node represents whether through siRNA it was identified as a cell-sorting target (red) or not (blue). The arrows represent the strength of the information flow within the network and the intensity is proportional to the modulation of the pTyr site involved in the specific edge. Arrows color-coded red represent an interaction supported by the contextual protein association network. Different kinases between the EphB2$^+$ and ephrin-B1$^+$ cells appear to be responsible for the change in information flow, and it appears that SH2- and PTB-binding proteins are used to a larger degree in EphB2$^+$ cells than in ephrin-B1$^+$ cells. Only a subset of the network is shown; for the full network, see the SOM.

Tool for the Retrieval of Interacting Genes/Proteins (STRING) resource (*30*) so as to create a probabilistic high-confidence protein-protein interaction network. Thus, by applying stringent filters we generated a cell-specific model of information processing during bidirectional signaling between mixed EphB2$^+$ and ephrin-B1$^+$ cells (Fig. 5).

Cell-specific signal processing in Eph receptor and ephrin signaling networks. To reflect the flow of information through pTyr sites, we assembled cell-specific networks in a modular fashion so that kinases (top layer) were connected through pTyr sites (middle layer) to phospho-binding modules (bottom layer) (Fig. 5). The signal strength through the connected kinases, pTyr sites, and phospho-binding modules is reflected by the modulation of the individual pTyr sites and represented by the intensity of the line (indicating an interaction) (Fig. 5).

Previously characterized pTyr-dependent protein-protein interactions involved in regulating cytoskeletal rearrangement and cell migration were confirmed by the model (Fig. 5). For example, phosphorylated EPHB2 displays increased interaction with RASA1 and DOK1 after EphR activation (*31*). Phosphorylation of Y428 on SHC1 creates a well-described binding site for the adaptor protein GRB2 after activation of receptor tyrosine kinases (RTKs) (*32*). Association between cortactin (CTTN, Y384) and the tyrosine kinase FER is important for subsequent phosphorylation and regulation of CTTN function in cell-cell signaling (*33*). As well, an interaction between tyrosine-phosphorylated p190RhoGAP (GRFL1) and RASA1 regulates cellular migration (*34*). Previously undescribed pTyr-dependent interactions are also suggested by the model, such as interactions between tyrosine-phosphorylated EPHB2 and the SH2 domain of the adaptor protein SHB and the tyrosine-phosphorylated SHB with the SH2 domain of RASA1.

A global comparison of cell-specific signaling networks suggests that asymmetric regulation of tyrosine phosphorylation events between EphB2$^+$ and ephrin-B1$^+$ cells is achieved through alternative use of kinases and adaptor proteins, thereby providing alternative signaling paths to relay information. Most of the pTyr signaling in EphB2$^+$ cells originates from the EPHB2 and ABL1 kinases, with NCK1, PXN, DOK1, and SHB as predicted direct targets (Fig. 5). Conversely, in ephrin-B1$^+$ cells, the insulin-like growth factor receptor (IGF1R) is predicted to initiate some of the pTyr signaling, which is in agreement with the observation that both the activation loop (Y1161) of IGF1R and its target IRS2 display increased tyrosine phosphorylation in ephrin-B1$^+$ cells after stimulation. Currently, we cannot exclude the possibility that other tyrosine kinases contribute to the observed pTyr regulation. Although other possible kinases were predicted for the positively modulated pTyr sites, we only obtained experimental evidence of increased activation loop phosphorylation for IGF1R and PTK2 in ephrin-B1$^+$ cells.

Consistent with SH2 and PTB domain–containing proteins displaying differential phosphorylation in EphB2$^+$ and ephrin-B1$^+$ cells (Fig. 2B), the network model shows asymmetric utilization of adaptor proteins. For example, several of the direct targets predicted for EPHB2 and ABL1 contain a pTyr binding module (SH2 or PTB), whereas less information is processed through the phosphorylation of SH2 and PTB domain–containing proteins in ephrin-B1$^+$ cells. SHB, an adaptor protein that has not previously been characterized with respect to EphR-ephrin signaling, appears to relay information from EPHB2 to CRK, RASA1, and PIK3R1. The asymmetric modulation of SHB tyrosine phosphorylation, coupled with the inhibitory effects of SHB siRNA on cell sorting, support the prediction that SHB may act as a crucial signal integrator (Figs. 3B and 5).

The global comparison of pTyr modulation in ephrin-B1$^+$ and EphB2$^+$ cells showed that a similar number of pTyr sites display negative or positive modulation (fig. S5A). Consistent with this observation, the network model identified several tyrosine phosphatases that may have a role in balancing pTyr signaling. Although tyrosine phosphatases have been described in EphR-ephrin signaling (*17*, *35*–*37*), the model implicates protein tyrosine phosphatase (PTP) non-receptor type 6 (PTPN6) and PTP receptor type A (PTPRA) as previously undescribed regulators of this process in addition to PTPN11, which has been linked to EphA receptor signaling. PTPN6 and PTPN11, which according to the network model are in close proximity to EPHB2, were identified in the siRNA screen, and PTPN11 phosphorylation (Y62) was modulated in an EphB2$^+$ cell–specific manner, suggesting that these phosphatases probably function in EphB2 and ephrin-B1 signaling and cell sorting.

Lastly, when comparing the signaling network models with the siRNA screen, we observed a strong bias toward highly connected signaling proteins exhibiting an siRNA phenotype (P = 0.001 for EphB2$^+$ cells and P = 0.002 for ephrin-B1$^+$ cells; Wilcoxon test) (fig. S10) (*18*).

Signaling abilities of Eph and ephrin intracellular region. Ephrin-B1, lacking its cytoplasmic region, retains the ability to initiate signaling through a B-type EphR on a neighboring cell but lacks intrinsic signaling properties and thus only elicits a unidirectional signal (Fig. 6A) (*4*). The size of the signaling cluster established between interacting EphRs and ephrins can markedly affect receptor activation and signaling (*36*), and so the intracellular region of ephrin-B1 might affect the strength or quality of the signal within the EphB2-expressing cell through its ability to associate with SH2 or PDZ domain–containing proteins.

To systematically study this, we engineered HEK293 cells to express a variant of ephrin-B1 lacking the cytoplasmic tail (ephrin-B1ΔIC$^+$) and selected cells with a similar level of surface expression as that observed in ephrin-B1$^+$ cells (fig. S1) (*18*). We then mixed EphB2$^+$ cells with either ephrin-B1ΔIC$^+$ cells or ephrin-B1$^+$ cells (expressing wild-type ephrin-B1) and used qBidS to compare their sorting phenotypes and the resulting pTyr signals. This revealed that the intracellular tail of ephrin-B1 is required for proper cell sorting and also influences pTyr signaling in EphB2$^+$ cells (Fig. 6B and figs. S7 and S11) (*18*). Specifically, pTyr sites in EphB2$^+$ cells were differentially modulated depending on whether the EphB2$^+$ cells were stimulated with ephrin-B1ΔIC$^+$ or ephrin-B1$^+$ cells ($P = 9 \times 10^{-19}$; Wilcoxon test) (fig. S12B), indicating that the intracellular region of ephrin-B1 affects EphB2 signaling. For example, cofilin 1 [CFL-1 (Y139 and Y84)], EPHB2 (Y596/Y602), PARD3 (Y388 and Y1127), PXN (Y118), and PTK2 (Y576) were differently phosphorylated in EphB2$^+$ cells depending on the presence or absence of the cytoplasmic region of ephrin-B1 ($P < 0.05$; Wilcoxon test) (fig. S11). The qBidS approach can therefore identify and quantitate differences in signaling events in a target cell that result from alterations in a distinct signal-initiating cell (thus, a non–cell-autonomous effect).

We also observed major differences in the structure and utilization of the signaling network in EphB2$^+$ cells depending on whether they were mixed with ephrin-B1$^+$ or ephrin-B1ΔIC$^+$ cells (Fig. 6B). Nodes and edges in the EphB2$^+$ cell signaling network that are influenced by the cytoplasmic tail of ephrin-B1 are depicted in a color-coded scheme, and those that were utilized similarly are in gray. The information flow from all predicted kinases and nearly all phospho-binding domains was affected when EphB2$^+$ cells were mixed with ephrin-B1ΔIC$^+$ cells as

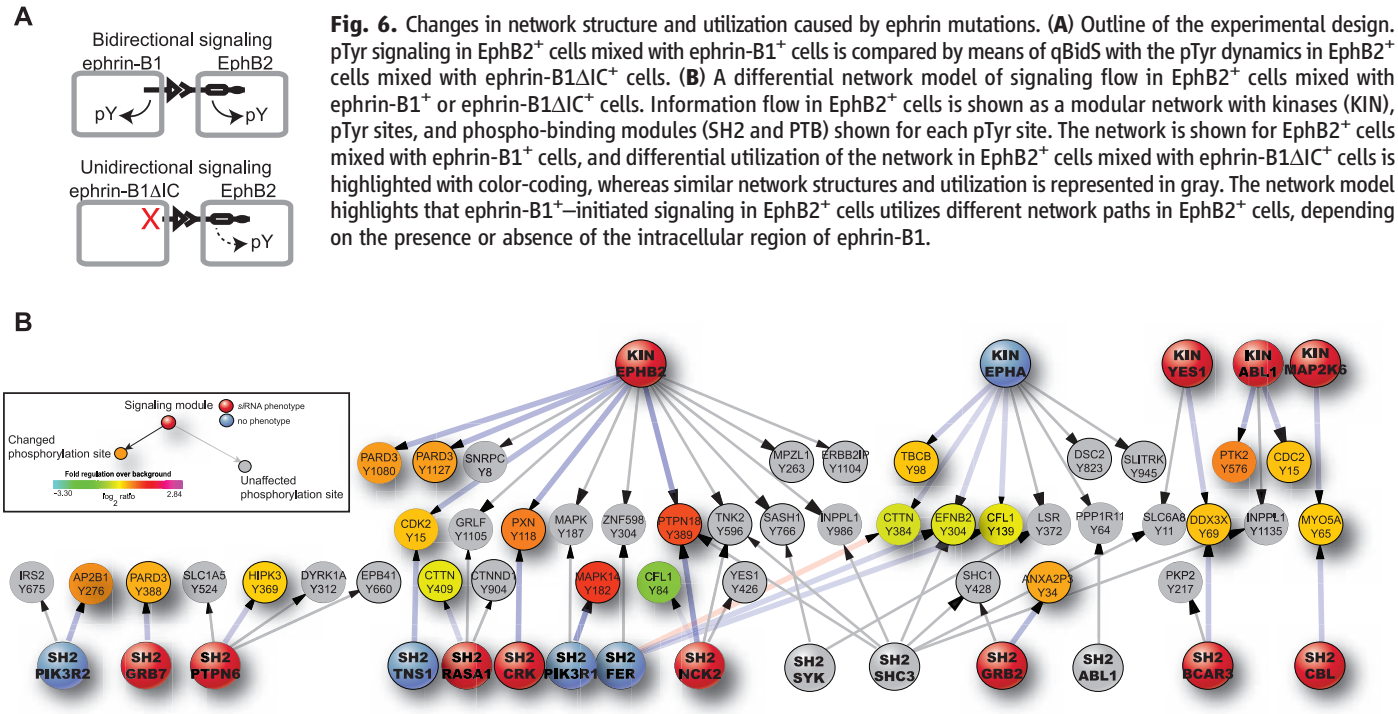

Fig. 6. Changes in network structure and utilization caused by ephrin mutations. (**A**) Outline of the experimental design. pTyr signaling in EphB2$^+$ cells mixed with ephrin-B1$^+$ cells is compared by means of qBidS with the pTyr dynamics in EphB2$^+$ cells mixed with ephrin-B1ΔIC$^+$ cells. (**B**) A differential network model of signaling flow in EphB2$^+$ cells mixed with ephrin-B1$^+$ or ephrin-B1ΔIC$^+$ cells. Information flow in EphB2$^+$ cells is shown as a modular network with kinases (KIN), pTyr sites, and phospho-binding modules (SH2 and PTB) shown for each pTyr site. The network is shown for EphB2$^+$ cells mixed with ephrin-B1$^+$ cells, and differential utilization of the network in EphB2$^+$ cells mixed with ephrin-B1ΔIC$^+$ cells is highlighted with color-coding, whereas similar network structures and utilization is represented in gray. The network model highlights that ephrin-B1$^+$–initiated signaling in EphB2$^+$ cells utilizes different network paths in EphB2$^+$ cells, depending on the presence or absence of the intracellular region of ephrin-B1.

opposed to ephrin-B1$^+$ cells. For example, whereas the predicted kinase for some pTyr sites such as PARD3 (Y1127) remained unaltered, other pTyr sites such as CTTN (Y384), PARD3 (Y1080), and PXN (Y118) were predicted to be modulated by an alternative kinase, suggesting that the dynamics and structure of the EphB2 signaling network is significantly influenced by the intracellular region of ephrin-B1 (Fig. 6D) [detailed networks are available in the supporting online material (SOM)].

Taken together, these data show that the intracellular region of ephrin-B1 affects signal processing not only within ephrin-B1$^+$ cells but also in neighboring cells that express EphB2, revealing a non–cell-autonomous mode of regulation in EphR-ephrin signaling. The same applies to the C-terminal valine of ephrin-B1 required for PDZ domain–binding of ephrin-B1, which also influenced signaling in EphB2$^+$ cells (fig. S13) (*18*). Furthermore, pTyr signaling is differently modulated in EphB2$^+$ cells depending on whether they are mixed with ephrin-B1ΔIC$^+$ or ephrin-B1ΔV$^+$ cells (Fig. 6 and figs. S11 and S13), suggesting that additional components besides PDZ domain–containing proteins may be required to orchestrate the signaling effects of ephrin-B1 on EphB2. The cytoplasmic region of EphB2 influences signaling in ephrin-B1$^+$ cells (fig. S14). We observed a significantly different pTyr-signaling response when EphB2$^+$ or ephrin-B1$^+$ cells were stimulated by soluble fusion proteins containing the extracellular regions of ephrin-B1 or EphB2, respectively, as compared with coculture (figs. S5, S15, and S16) (*18*).

Discussion. We developed proteomic and computational approaches to identify cell-specific signaling networks in two cell populations as they contact one another and explored the phenotypic impact of these networks on cell sorting. Our models show that cell segregation requires the integration of multiple cellular processes. We found that information processing between EphB2$^+$ and ephrin-B1$^+$ cells is asymmetric and that there are both structural and dynamic differences in the networks mediating the molecular information flow induced by bidirectional signaling on the one hand, as compared with unidirectional signaling induced either by C-terminally truncated cell surface ligands, or soluble proteins on the other. One aim of integrative network biology is to model biological systems with an accuracy and predictive power similar to that of other physical systems, and thus it is essential to intertwine quantitative measurements of cell behavior and signaling dynamics through computational modeling (*16*, *38*, *39*–*41*). The availability of more diverse and larger quantitative phenotypic, proteomic, and interaction data, with improved algorithms (*26*, *27*, *38*), will enable more accurate and elaborate signaling models to be generated. The systems-level approaches described here are of general utility in studying the effects of cell-cell interactions and network utilization in both normal and pathologic processes.

References and Notes

1. J. Downward, *Nature* **411**, 759 (2001).
2. M. V. Gelfand, S. Hong, C. Gu, *Trends Cell Biol.* **19**, 99 (2009).
3. M. Henkemeyer *et al.*, *Cell* **86**, 35 (1996).
4. G. Mellitzer, Q. Xu, D. G. Wilkinson, *Nature* **400**, 77 (1999).
5. E. Batlle *et al.*, *Cell* **111**, 251 (2002).
6. M. Lackmann, A. W. Boyd, *Sci. Signal.* **1**, re2 (2008).
7. S. J. Holland *et al.*, *Nature* **383**, 722 (1996).
8. K. Brückner, E. B. Pasquale, R. Klein, *Science* **275**, 1640 (1997).
9. A. Davy *et al.*, *Genes Dev.* **13**, 3125 (1999).
10. D. Lin, G. D. Gish, Z. Songyang, T. Pawson, *J. Biol. Chem.* **274**, 3726 (1999).
11. K. Brückner *et al.*, *Neuron* **22**, 511 (1999).
12. D. Arvanitis, A. Davy, *Genes Dev.* **22**, 416 (2008).
13. C. Cortina *et al.*, *Nat. Genet.* **39**, 1376 (2007).
14. E. B. Pasquale, *Nat. Rev. Mol. Cell Biol.* **6**, 462 (2005).
15. K. A. Janes *et al.*, *Science* **310**, 1646 (2005).
16. K. Miller-Jensen, K. A. Janes, J. S. Brugge, D. A. Lauffenburger, *Nature* **448**, 604 (2007).
17. A. Poliakov, M. L. Cotrina, A. Pasini, D. G. Wilkinson, *J. Cell Biol.* **183**, 933 (2008).
18. Materials and methods are available as supporting material on *Science* Online.
19. S.-E. Ong *et al.*, *Mol. Cell. Proteomics* **1**, 376 (2002).
20. Y. Oda, K. Huang, F. R. Cross, D. Cowburn, B. T. Chait, *Proc. Natl. Acad. Sci. U.S.A.* **96**, 6591 (1999).
21. Single-letter abbreviations for the amino acid residues are as follows: A, Ala; C, Cys; D, Asp; E, Glu; F, Phe; G, Gly; H, His; I, Ile; K, Lys; L, Leu; M, Met; N, Asn; P, Pro; Q, Gln; R, Arg; S, Ser; T, Thr; V, Val; W, Trp; and Y, Tyr.
22. Y. Zhang *et al.*, *Mol. Cell. Proteomics* **4**, 1240 (2005).
23. J. Rush *et al.*, *Nat. Biotechnol.* **23**, 94 (2005).
24. C. J. Echeverri, N. Perrimon, *Nat. Rev. Genet.* **7**, 373 (2006).
25. B. T. Seet, I. Dikic, M.-M. Zhou, T. Pawson, *Nat. Rev. Mol. Cell Biol.* **7**, 473 (2006).
26. C. Jørgensen, R. Linding, *Brief. Funct. Genomics Proteomics* **7**, 17 (2008).
27. A. Gordus *et al.*, *Mol. Syst. Biol.* **5**, 235 (2009).
28. R. Linding *et al.*, *Cell* **129**, 1415 (2007).
29. M. L. Miller *et al.*, *Sci. Signal.* **1**, ra2 (2008).
30. C. von Mering *et al.*, *Nucleic Acids Res.* **31**, 258 (2003).
31. S. J. Holland *et al.*, *EMBO J.* **16**, 3877 (1997).
32. M. Rozakis-Adcock *et al.*, *Nature* **360**, 689 (1992).
33. L. Kim, T. W. Wong, *J. Biol. Chem.* **273**, 23542 (1998).
34. J. McGlade *et al.*, *EMBO J.* **12**, 3073 (1993).
35. T. Shintani *et al.*, *Nat. Neurosci.* **9**, 761 (2006).
36. E. Stein *et al.*, *Genes Dev.* **12**, 667 (1998).
37. H. Miao, E. Burnett, M. Kinch, E. Simon, B. Wang, *Nat. Cell Biol.* **2**, 62 (2000).
38. K. A. Janes, M. B. Yaffe, *Nat. Rev. Mol. Cell Biol.* **7**, 820 (2006).
39. C. Bakal *et al.*, *Science* **322**, 453 (2008).
40. C. S. H. Tan *et al.*, *Science* **325**, 1686 (2009).
41. C. S. H. Tan *et al.*, *Science Signal.* **2**, ra39 (2009).

42. We thank C. Bakal, J. Erler, C. Marshall, R. Marais (ICR), and K. Colwill (SLRI) for critical input on this manuscript. The authors are further indebted to O. Rocks, A. James, V. Nguyen, R. Bagshaw, A.-C. Gingras (SLRI), P. Huang (ICR), L. Foster (University of British Columbia), L. J Jensen (Center for Protein Research), S. Tate (Applied Biosystems/Sciex), and Thermo Scientific (in particular A. Sullivan) for technical assistance. This project was supported by Genome Canada through the Ontario Genomics Institute, a Terry Fox Programme grant from the Canadian Cancer Society, the Canadian Institutes for Health Research (grant MOP-6849), the Canada Foundation for Innovation, the Human Frontiers Science Program, and The Lundbeck Foundation. C.J. conceived and implemented the qBidS approach. R.L. conceived and performed the modeling work. C.J, A.S., and T.P. conceived and designed the siRNA screen. D.G.W. and A.P. (MRC NIMR) provided cell lines and advice on cell sorting. C.J., A.S., G.I.C., M.H., and B.L. conceived, designed, and performed the experiments. A.P., C.J., and R.L. conceived, designed, and performed the computational experiments. T.P. and R.L. oversaw the project. C.J., R.L., and T.P. wrote the paper. Mass spectrometric data has been submitted to the Proteomics Identifications (PRIDE) database under accession numbers 10295–10296. Identified phosphorylation sites have also been submitted to the Phospho-ELM and PhosphoSite databases.

Supporting Online Material
www.sciencemag.org/cgi/content/full/326/5959/1502/DC1
Materials and Methods
SOM Text
Figs. S1 to S21
Tables S1 to S5
References

21 May 2009; accepted 1 October 2009
10.1126/science.1176615

Breaking the Code of DNA Binding Specificity of TAL-Type III Effectors

Jens Boch,* Heidi Scholze, Sebastian Schornack,† Angelika Landgraf, Simone Hahn, Sabine Kay, Thomas Lahaye, Anja Nickstadt,‡ Ulla Bonas

The pathogenicity of many bacteria depends on the injection of effector proteins via type III secretion into eukaryotic cells in order to manipulate cellular processes. TAL (transcription activator–like) effectors from plant pathogenic *Xanthomonas* are important virulence factors that act as transcriptional activators in the plant cell nucleus, where they directly bind to DNA via a central domain of tandem repeats. Here, we show how target DNA specificity of TAL effectors is encoded. Two hypervariable amino acid residues in each repeat recognize one base pair in the target DNA. Recognition sequences of TAL effectors were predicted and experimentally confirmed. The modular protein architecture enabled the construction of artificial effectors with new specificities. Our study describes the functionality of a distinct type of DNA binding domain and allows the design of DNA binding domains for biotechnology.

Phytopathogenic bacteria of the genus *Xanthomonas* cause severe diseases on many crop plants. Pathogenicity relies on the translocation of effector proteins into the plant cell cytoplasm via the type III secretion system (*1*–*5*). Members of the large transcription activator-like (TAL) effector family are key virulence factors of *Xanthomonas* (*4*–*7*) and reprogram host cells by mimicking eukaryotic transcription factors (*8*–*13*). TAL effector–mediated gene induction leads to plant developmental changes [for example, cell divisions and cell enlargement such as citrus canker and hypertrophy (*4*)], thus contributing to disease symptoms. Although a number of plant targets, including susceptibility genes, have been identified (*8*–*10*, *12*–*14*), the targets of most TAL effectors have not been elucidated.

TAL effectors are characterized by a central domain of tandem repeats, nuclear localization signals (NLSs), and an acidic transcriptional activation domain (AD) (Fig. 1A) (*11*, *15*, *16*). Members of this effector family are highly conserved and differ mainly in the amino acid sequence and number of repeats. The number and order of repeats in a TAL effector determine its specific activity (*17*, *18*). The type member of this effector family, AvrBs3 from *Xanthomonas campestris* pv. *vesicatoria*, contains 17.5 repeats and induces expression of *UPA* (upregulated by AvrBs3) genes, including the *Bs3* resistance gene in pepper plants (*9*, *10*, *14*, *19*). The repeats of AvrBs3 are essential for DNA binding of AvrBs3 and represent a distinct type of DNA binding domain (*9*). How this domain contacts DNA and what determines specificity has remained enigmatic so far.

A model for sequence specificity. The fact that AvrBs3 directly binds to the *UPA* box, a promoter element in induced target genes (*9*, *10*), prompted us to investigate the basis for DNA-sequence specificity. The repeat region of AvrBs3 consists of 34 amino acid repeat units that are nearly identical; however, amino acids 12 and 13 are hypervariable (Fig. 1A) (*11*). The most C-terminal repeat of AvrBs3 shows a sequence similarity to other repeats only in its first 20 amino acids and is therefore referred to as a half repeat. The repeats can be classified into different repeat types on the basis of their hypervariable 12th and 13th amino acids (Fig. 1B). Because the size of the *UPA* box [18 base pairs (bp) (*20*)

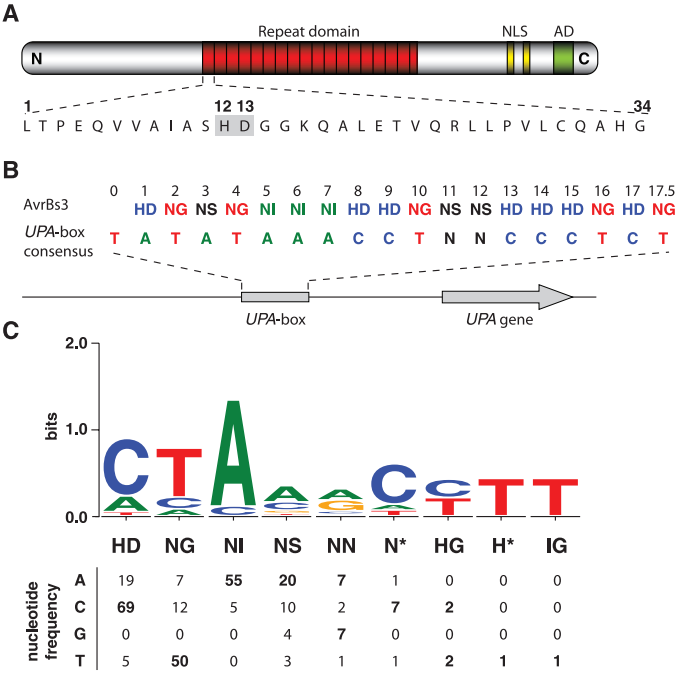

Fig. 1. Model for DNA-target specificity of TAL effectors. (**A**) TAL effectors contain central tandem repeats, NLSs, and an AD. Shown is the amino acid sequence of the first repeat of AvrBs3. Hypervariable amino acids 12 and 13 are shaded in gray. (**B**) Hypervariable amino acids at position 12 and 13 of the 17.5 AvrBs3 repeats are aligned to the *UPA* box consensus (*14*). (**C**) Repeats of TAL effectors and predicted target sequences in promoters of induced genes were aligned manually. Nucleotides in the upper DNA strand that correspond to the hypervariable amino acids in each repeat were counted on the basis of the following combinations of eight effectors and experimentally identified target genes: AvrBs3/*Bs3*, *UPA10*, *UPA12*, *UPA14*, *UPA19*, *UPA20*, *UPA21*, *UPA23*, *UPA25*, AvrBs3Δrep16/*Bs3-E*, AvrBs3Δrep109/*Bs3*, AvrHah1/*Bs3*, AvrXa27/*Xa27*, PthXo1/*Xa13*, PthXo6/*OsTFX1*, and PthXo7/*OsTFIIAγ1* (fig. S1). An asterisk indicates that amino acid 13 is missing in this repeat type. Highest nucleotide frequencies are in bold. Nucleotide frequencies are displayed in a logo (http://weblogo.threeplusone.com).

Department of Genetics, Institute of Biology, Martin-Luther-University Halle-Wittenberg, Weinbergweg 10, D-06099 Halle (Saale) Germany.

*To whom correspondence should be addressed. E-mail: jens.boch@genetik.uni-halle.de
†Present address: Sainsbury Laboratory, John Innes Centre, Norwich, Norfolk NR4 7UH, UK.
‡Present address: Icon Genetics GmbH, Biozentrum, Weinbergweg 22, D-06120 Halle (Saale), Germany.